

Quantum squeezing induced nonreciprocal phonon laser

Tian-Xiang Lu,^{1,2} Yan Wang,³ Keyu Xia,⁴ Xing Xiao,¹ Le-Man Kuang,^{2,3} and Hui Jing^{2,3,*}

¹College of Physics and Electronic Information, Gannan Normal University, Ganzhou 341000, Jiangxi, China

²Key Laboratory of Low-Dimensional Quantum Structures and Quantum Control of Ministry of Education, Department of Physics and Synergetic Innovation Center for Quantum Effects and Applications, Hunan Normal University, Changsha 410081, China

³Academy for Quantum Science and Technology, Zhengzhou University of Light Industry, Zhengzhou 450002, China

⁴College of Engineering and Applied Sciences, National Laboratory of Solid State Microstructures, and Collaborative Innovation Center of Advanced Microstructures, Nanjing University, Nanjing 210023, China

(Dated: December 13, 2023)

Phonon lasers or coherent amplifications of mechanical oscillations have provided powerful tools for both fundamental studies of coherent acoustics and diverse applications ranging from ultrasensitive force sensing to phononic information processing. Here, we propose how to achieve directional phonon lasing with an optomechanical resonator coupled to a nonlinear optical resonator. We find that, by pumping the nonlinear resonator, directional optical squeezing can occur along the pump direction. As a result, we can achieve the directional mechanical gain by utilizing the directional optical squeezing, thus leading to nonreciprocal phonon lasing with a well-tunable directional power threshold. Our work shows a feasible way to build nonreciprocal phonon lasers with various nonlinear optical mediums, which are important for such a wide range of applications as directional acoustic amplifiers, invisible sound sensing or imaging, and one-way phononic networks.

I. INTRODUCTION

Phonon lasers or coherent amplifications of mechanical oscillations have played an essential role in the fundamental studies of coherent acoustics and applications ranging from sound imaging or sensing [1–5] to topological motion control [6] and phononic engineering [7, 8]. In recent years, phonon lasers have been achieved in diverse platforms, such as trapped ions [9, 10], cold atoms [11], optical tweezers [12, 13], and cavity optomechanical (COM) systems [14–19], to name only a few [20–25]. In particular, COM devices [26], suitable for integration on chip-scales, have been used to realize different kinds of phonon lasers [27–35], such as exceptional-point phonon lasers [27–29], phase-modulated phonon lasers [30, 31], and vector phonon lasers [32, 33].

Very recently, nonreciprocal phononic devices, featuring directional flow of phonons, were explored and utilized for chiral phonon transport or cooling [36–38], phonon isolation [39–44], one-way mechanical networks [45–51], and backscattering-immune acoustic sensing or imaging [52, 53]. In these works, nonreciprocal acoustic control has been enabled by incorporating nonlinear mediums [40–45], circulating fluids [39], macroscopic metamaterials [46–49], space-time modulations [54, 55], and complicated synthetic structures [51]. In particular, nonreciprocal phonon lasers were proposed by using the relativistic Sagnac effect in a spinning COM device or magnomechanical system [56, 57], making it possible to operate phonon lasers in a highly asymmetric way. However, in these works [56, 57], high-speed rotation of resonators is required and thus strongly relies on stable couplings between spinning devices and flying fibers. It is therefore highly desirable to seek a new approach that is free of any spinning component and easily tunable in optical ways.

In a very recent work, directional quantum squeezing was proposed to achieve an optical diode or circulator [58], opening up an attractive route to achieve nonreciprocal devices via harnessing various quantum resources. We note that the advantages of quantum squeezing have also been confirmed, e.g., significant amplifications of light-motion interactions or coherent couplings of hybrid quantum systems [59–78]. Based on one-way squeezing, nonreciprocal photonic or magnonic devices have also been explored [79–82]. Inspired by these pioneering works, here we study how to achieve a nonreciprocal phonon laser in a compound COM system by using directional optical squeezing. We find that by unidirectionally driving the nonlinear optical resonator, asymmetric coupling of the resonators can emerge, resulting in nonreciprocal mechanical gains and well-tunable direction-dependent threshold of phonon lasing. Also, we find that in such nonreciprocal devices, the mechanical gain exhibits squeezing-enhanced robustness against optical decays. Our scheme, requiring only two-mode optical-frequency matching and free of any spinning device, is promising to be realized under current experimental conditions and thus can be utilized for, e.g., nonreciprocal force sensing and chiral acoustic information processing or networking [36, 37].

II. THEORETICAL MODEL

As shown in Fig. 1, we consider a compound COM system consisting of two coupled whispering-gallery-mode (WGM) microtoroid resonators and two nearby optical waveguides. The resonator R_1 of resonance frequency ω_a and decay rate κ_1 supports a mechanical breathing mode (with frequency ω_m and effective mass m), and is driven by a signal field of frequency ω_l from port 1 (or port 2) corresponding to the forward-input case (or backward-input case). The other resonator R_2 of resonance frequency ω_a and decay rate κ_2 , manufactured of high-quality thin film with $\chi^{(2)}$ -nonlinearity [83–

* jinghui73@gmail.com

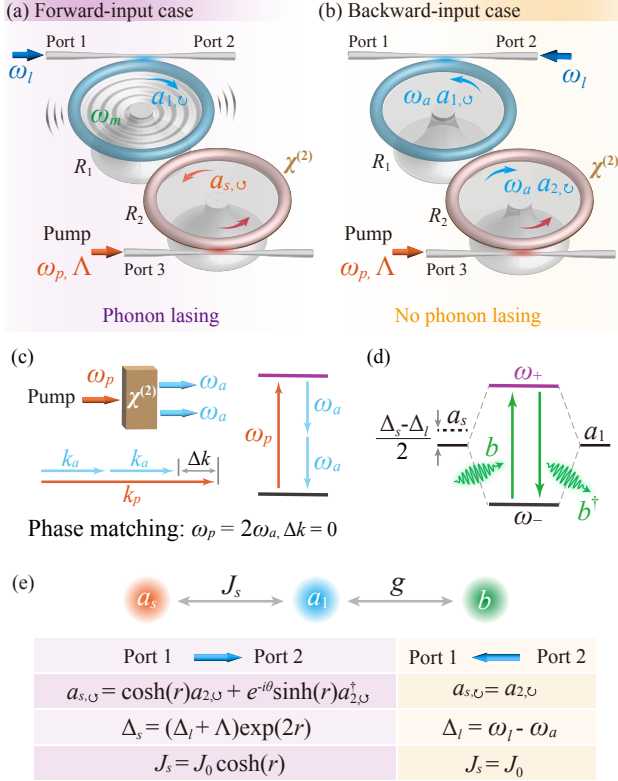


FIG. 1. (Color online) Operating a nonreciprocal phonon laser with directional squeezing. A strong pump with frequency ω_p and strength Λ , coming from port 3, causes the CCW mode to be squeezed, i.e., $a_{2,\odot} \rightarrow a_{s,\odot}$, in the nonlinear resonator R_2 . (a) The input laser with frequency ω_l driven from port 1 excites the CW mode $a_{1,\odot}$ in R_1 , which is coupled to the squeezed mode $a_{s,\odot}$ in R_2 with an effective strength J_s , while as shown in (b), when driven from port 2, it excites the CCW mode $a_{1,\odot}$ in R_1 , coupled to the non-squeezed mode $a_{2,\odot}$ in R_2 with the strength J_0 . (c) The nonlinear parametric process: a pump photon with frequency ω_p and wave-number k_p can be down-converted into two photons with the same frequency ω_a and wave-number k_a due to the $\chi^{(2)}$ nonlinearity under the phase matching condition. (d) The energy-level diagram shows the mechanism of two-level phonon laser, i.e., stimulated emissions of phonons under the condition of population inversion (for the optical supermodes ω_{\pm}). (e) The mode couplings of this system, with a comparison of direction-dependent key symbols. Here r is the squeezing parameter.

94], and thus supporting the parametric amplification process [59], is pumped from port 3 by a continuous coherent laser field with frequency ω_p , strength Λ , and phase θ . As shown in Fig. 1(c), because of the directional phase-matching condition in the parametric nonlinear process [58, 91], that is, the conservation of energy and momentum ($\omega_p = 2\omega_a$, $\Delta k = 0$), the counterclockwise (CCW) mode $a_{2,\odot}$ is squeezed to a mode $a_{s,\odot}$, but the clockwise (CW) mode $a_{2,\odot}$ is unsqueezed [58, 79, 80, 82]. For the forward-input case, in a frame rotating at frequency ω_l , the total Hamiltonian of the

system can be written at the simplest level as ($\hbar = 1$):

$$\begin{aligned} \mathcal{H} = & -\Delta_l a_{1,\odot}^\dagger a_{1,\odot} - \Delta_l a_{2,\odot}^\dagger a_{2,\odot} + \omega_m b^\dagger b, \\ & + J_0 (a_{1,\odot}^\dagger a_{2,\odot} + a_{2,\odot}^\dagger a_{1,\odot}) - g x_0 a_{1,\odot}^\dagger a_{1,\odot} (b + b^\dagger), \\ & + i\varepsilon_l (a_{1,\odot}^\dagger - a_{1,\odot}) + \frac{\Lambda}{2} (a_{2,\odot}^{\dagger 2} e^{-i\theta} + a_{2,\odot}^2 e^{i\theta}), \end{aligned} \quad (1)$$

where $a_{1,\odot}$ ($a_{1,\odot}^\dagger$), $a_{2,\odot}$ ($a_{2,\odot}^\dagger$), and b (b^\dagger) are the annihilation (creation) operators of the CW mode in R_1 , the CCW mode in R_2 , and the mechanical mode in R_1 , respectively. $\Delta_l = \omega_l - \omega_a$, J_0 (or $g = \omega_a/r_1$) denotes the coupling strength between the resonators (or the COM coupling strength), $x_0 = \sqrt{\hbar/2m\omega_m}$, and r_1 is the radius of the COM resonator. $\varepsilon_l = \sqrt{2\kappa_1 P_{\text{in}}/\hbar\omega_l}$ is the driving amplitude with input power P_{in} . To diagonalize \mathcal{H} , we define the squeezed operator $a_{s,\odot}$ via the Bogoliubov transformation [59, 61]:

$$a_{s,\odot} = \cosh(r)a_{2,\odot} + e^{-i\theta}\sinh(r)a_{2,\odot}^\dagger, \quad (2)$$

with the squeezing parameter $r = (1/4)\ln[(\Delta_l - \Lambda)/(\Delta_l + \Lambda)]$, which requires $|\Delta_l| > |\Lambda|$ to avoid the system instability. Then, with the rotating wave approximation (see Appendix A for more details), the Hamiltonian of the system becomes

$$\begin{aligned} \mathcal{H}_f = & -\Delta_l a_{1,\odot}^\dagger a_{1,\odot} - \Delta_s a_{s,\odot}^\dagger a_{s,\odot} + J_s (a_{1,\odot}^\dagger a_{s,\odot} + a_{s,\odot}^\dagger a_{1,\odot}) \\ & + \omega_m b^\dagger b - g x_0 a_{1,\odot}^\dagger a_{1,\odot} (b + b^\dagger) + i\varepsilon_l (a_{1,\odot}^\dagger - a_{1,\odot}), \end{aligned} \quad (3)$$

where

$$\Delta_s = (\Delta_l + \Lambda)\exp(2r), \quad J_s = J_0 \cosh(r). \quad (4)$$

It is clearly seen that the effective squeezed mode detuning Δ_s and the effective coupling rate J_s are modulated by the squeezing strength Λ under the condition of ensuring the stability of the system (e.g., $|\Delta_l| > |\Lambda|$). For the backward-input case, the Hamiltonian of the system reads

$$\begin{aligned} \mathcal{H}_b = & -\Delta_l a_{1,\odot}^\dagger a_{1,\odot} - \Delta_l a_{2,\odot}^\dagger a_{2,\odot} + J_0 (a_{1,\odot}^\dagger a_{2,\odot} + a_{2,\odot}^\dagger a_{1,\odot}) \\ & + \omega_m b^\dagger b - g x_0 a_{1,\odot}^\dagger a_{1,\odot} (b + b^\dagger) + i\varepsilon_l (a_{1,\odot}^\dagger - a_{1,\odot}). \end{aligned} \quad (5)$$

Comparing the Hamiltonians \mathcal{H}_f and \mathcal{H}_b , it can be clearly seen that the detuning and coupling strengths of these two Hamiltonians are completely different due to the directional squeezing effect.

Below, we show that for our COM system, this directional squeezing effect leads to distinct changes in the radiation pressure on the mechanical mode, hence resulting in a nonreciprocal phonon lasing action. Then, for the forward-input case, the steady-state solutions can be obtained as (see Appendix A for more details)

$$\begin{aligned} \alpha_{1,\odot} &= \frac{\varepsilon_l(\kappa_2 - i\Delta_s)}{(\kappa_1 - i\Delta_l - igx_s)(\kappa_2 - i\Delta_s) + J_s^2}, \\ \alpha_{s,\odot} &= \frac{J_s \alpha_{1,\odot}}{\Delta_s + i\kappa_2}, \quad \beta = \frac{gx_s |\alpha_{1,\odot}|^2}{\omega_m - i\gamma_m}, \end{aligned} \quad (6)$$

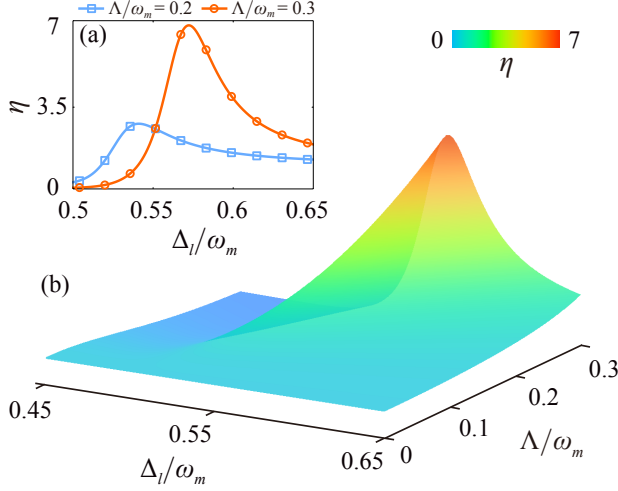


FIG. 2. (Color online) (a) The mechanical displacement amplification factor η as a function of the optical detuning Δ_l , for different values of squeezing strength Λ . (b) η versus Δ_l and Λ , with the experimentally accessible parameter values $J_0/\omega_m = 0.5$ and $P_{in} = 10 \mu W$.

where γ_m is the damping rate of the mechanical mode. In our calculations, for the backward-input case, we need to, respectively, replace $a_{1,\cup}$, $a_{s,\cup}$, J_s , Δ_s with $a_{1,\cup}$, $a_{2,\cup}$, J_0 , Δ_l . $x_s = x_0(\beta + \beta^*)$ is the steady-state mechanical displacement, and is proportional to

$$x_s = \frac{\hbar g |\alpha_{1,\cup}|^2}{m(\omega_m^2 + \gamma_m^2)}. \quad (7)$$

To see the effect of the squeezing effect on the radiation pressure of the mechanical mode, we defined the mechanical displacement amplification factor

$$\eta = \frac{x_s(\Lambda \neq 0)}{x_s(\Lambda = 0)}, \quad (8)$$

here $x_s(\Lambda \neq 0)$ [$x_s(\Lambda = 0)$] is the displacement corresponding to the forward-input case (backward-input case). Clearly, besides the driving field ε_l , the squeezing strength Λ also affects the values of the mechanical displacement x_s . For the forward-input case, both the effective coupling rate J_s and the effective squeezed mode detuning Δ_s , can be adjusted by the squeezing strength Λ . Figures 2(a) and 2(b) show the mechanical displacement amplification factor η as a function of the optical detuning Δ_l and the squeezing strength Λ . It is seen that the mechanical displacement amplification factor can be adjusted due to the squeezing effect, that is, the steady-state mechanical displacement x_s can be enhanced for the forward-input case. The amplified displacement indicates an enhancement of phonon generation [56, 57].

Now we will show that nonreciprocal phonon lasing action can be achieved in such a system. By use of the supermode operators [14–16]

$$a_{\pm} = (a_{1,\cup} \pm a_{s,\cup}) / \sqrt{2}, \quad (9)$$

the Hamiltonian of Eq. (3) can be written as

$$\begin{aligned} H = & \omega_+ a_+^\dagger a_+ + \omega_- a_-^\dagger a_- + \frac{\Delta}{2} (a_+^\dagger a_- + a_-^\dagger a_+) \\ & + \omega_m b^\dagger b - \frac{g x_0}{2} (a_+^\dagger a_- b + b^\dagger a_-^\dagger a_+) \\ & + \frac{i \varepsilon_l}{\sqrt{2}} [(a_+^\dagger + a_-^\dagger) - (a_+ + a_-)], \end{aligned} \quad (10)$$

after applying the rotating-wave approximation [14, 56, 57], where effective mode frequencies

$$\omega_{\pm} = -(\Delta_s + \Delta_l)/2 \pm J_s, \quad (11)$$

and $\Delta = \Delta_s - \Delta_l$. For the backward-input case, we have $\Delta = 0$ and $J_s = J_0$. We note that, compared with the traditional phonon laser system (absorption and emission of phonons are described by the fourth term) [14–16], Eq. (10) contains an additional detuning term (the third term). It implies that the coupling between the optical supermodes depends on the squeezing effect when driving the resonator from port 1. Thus, the phonon lasing process can be dramatically modified. Usually, the supermode operators are defined as $a_{\pm} = (a_{1,\cup} \pm a_{s,\cup}) / \sqrt{2}$ for coupled cavities with the same resonant frequency [14, 15, 56, 57, 82]. As mentioned earlier, the squeezing strength Λ has brought some changes to our system, such as the effective squeezed mode detuning Δ_s and the effective coupling rate J_s . According to Ref. [58], J_s is enhanced exponentially relative to J_0 with increasing Λ . However, in our work, to ensure that this transformation can safely be simplified as we use the above operators [derived from Eq. (3) to Eq. (10)], we do not consider the system to achieve strong coupling. Hence, the maximum value of squeezing strength is $0.3\omega_m$ in this work. For $\Lambda/\omega_m \leq 0.3$, we have confirmed that the detuning $\Delta = \Delta_s - \Delta_l$ and the enhanced coupling rate $\Delta J = J_s - J_0$ are much smaller than Δ_l and J_0 . For example, when $\Lambda/\omega_m = 0.3$, the detuning Δ/ω_m is about 0.1, and the enhanced coupling rate J_s/J_0 is about 1.05. These mean that our calculations are reasonable and valid.

By using the ladder operator and population-inversion operator of the optical supermodes as [14, 15]

$$p = a_-^\dagger a_+, \quad \delta n = a_+^\dagger a_+ - a_-^\dagger a_-, \quad (12)$$

respectively, the equations of motion of the system then become

$$\begin{aligned} \dot{b} = & -(\gamma_m + i\omega_m)b + \frac{igx_0}{2}p, \\ \dot{p} = & -2(\kappa_0 + iJ_s)p + \frac{i}{2}(\Delta - gx_0b)\delta n + \frac{\varepsilon_l}{\sqrt{2}}(a_+ + a_-^\dagger), \end{aligned} \quad (13)$$

where $\kappa_0 = (\kappa_1 + \kappa_2)/2$. By using the standard procedures (see Appendix B for more details), the mechanical gain G can be obtained:

$$\begin{aligned} G = G_0 + \mathcal{G} = & \frac{g^2 x_0^2 \kappa_0 \delta n}{2(2J_s - \omega_m)^2 + 8\kappa_0^2} \\ & + \frac{\varepsilon_l^2 g^2 x_0^2 (\omega_m - 2J_s)(\Delta_s + \Delta_l)\kappa_0}{[4(2J_s - \omega_m)^2 + 16\kappa_0^2][D^2 + (\Delta_l + \Delta_s)^2 \kappa_0^2]}, \end{aligned} \quad (14)$$

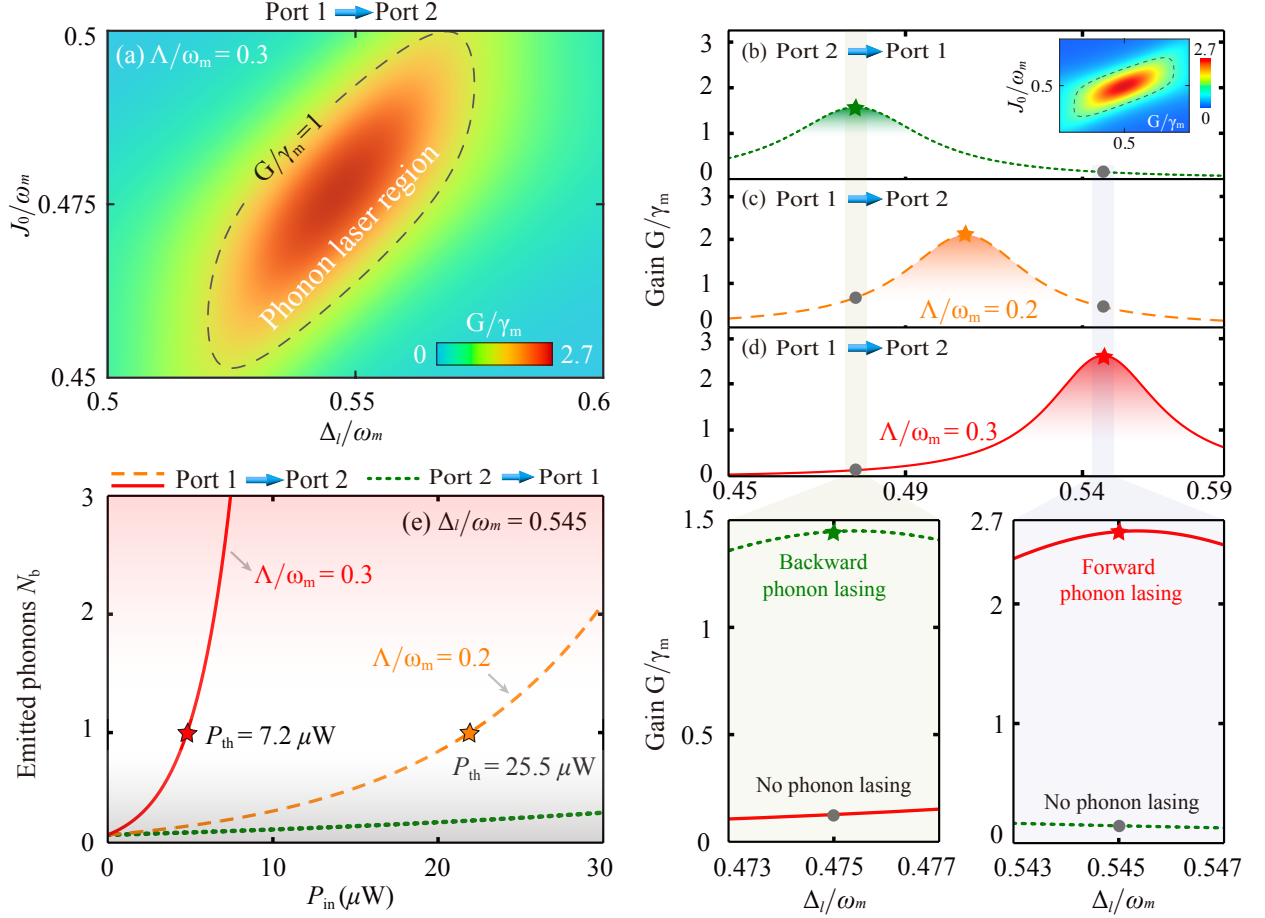


FIG. 3. (Color online) (a) The mechanical gain G versus the detuning Δ_l and the coupling strength J_0 for the forward-input case (port 1 \rightarrow port 2). (b-d) G versus Δ_l for different input directions. The right inset shows G versus Δ_l and J_0 for the backward-input case (port 2 \rightarrow port 1). Orange dashed and red solid curves correspond to the forward-input case for the squeezing strengths $\Lambda/\omega_m = 0.2$ and $\Lambda/\omega_m = 0.3$, respectively. The green dashed curve corresponds to the backward-input case with $\Lambda/\omega_m = 0.2$ and $\Lambda/\omega_m = 0.3$. (e) The stimulated emitted phonon number N_b as a function of the pump power P_{in} for different input directions. The five-pointed stars correspond to the threshold power P_{th} , which is determined by the threshold condition $G = \gamma_m$. We choose $P_{in} = 10 \mu\text{W}$ in (a-d), $J_0/\omega_m = 0.48$ in (b-d), and $\Delta_l/\omega_m = 0.545$ in (e).

with

$$D = J_s^2 + \kappa_0^2 - \Delta_s \Delta_l + \frac{[g^2 x_0^2 n_b - 2g x_0 \Delta \text{Re}(b)]}{4},$$

$$\delta n = \frac{\varepsilon_l^2 [2J_s \Delta_s - \kappa_0 g x_0 \text{Im}(b) - J_s g x_0 \text{Re}(b)]}{D^2 + \kappa_0^2 (\Delta_l + \Delta_s)^2}, \quad (15)$$

where $n_b = b^\dagger b$ is the phonon number. We note that the first term G_0 in Eq. (14) is proportional to the population inversion δn , and δn depends on Δ_s , which is quite different from the conventional phonon laser system without directional quantum squeezing effect. Also, the second term \mathcal{G} in Eq. (14) depends on Δ_s . This indicates that different mechanical gains can be obtained for the forward-input and backward-input cases, which makes it possible to achieve a nonreciprocal phonon laser.

III. NONRECIPROCAL PHONON LASER

In numerical simulations, to demonstrate that the observation of the phonon laser process is within current experimental reach, we have selected experimentally feasible parameters [14], i.e., $\omega_a = 1.93 \times 10^5$ GHz, the optical quality factor $Q_1 = 9.7 \times 10^7$, $Q_2 = 4 \times 10^7$, $\kappa_{1,2} = \omega_a/Q_{1,2}$, $2r_1 = 66 \mu\text{m}$, $2r_2 = 69 \mu\text{m}$, $\omega_m/2\pi = 23.4$ MHz, $m = 50$ ng, $\gamma_m = 0.24$ MHz, and $\Lambda/\omega_m = 0.3$, and thus $\Delta_l/\omega_m \sim 0.1$ and $J_s/J_0 \sim 1.05$.

In Fig. 3(a), the calculated mechanical gain G is plotted as a function of the optical detuning Δ_l and the coupling strength J_0 for the forward-input case. It is clearly shown that, for $\Lambda/\omega_m = 0.3$, the mechanical gain $G/\gamma_m > 1$ can be obtained with the proper selection of Δ_l and J_0 , making phonon lasing possible. A maximum mechanical gain of $G/\gamma_m \approx 2.7$ is obtained with $\Delta_l/\omega_m \sim 0.545$ and $J_0/\omega_m \sim 0.48$. This means that the strongest phonon lasing occurs due to the resonance

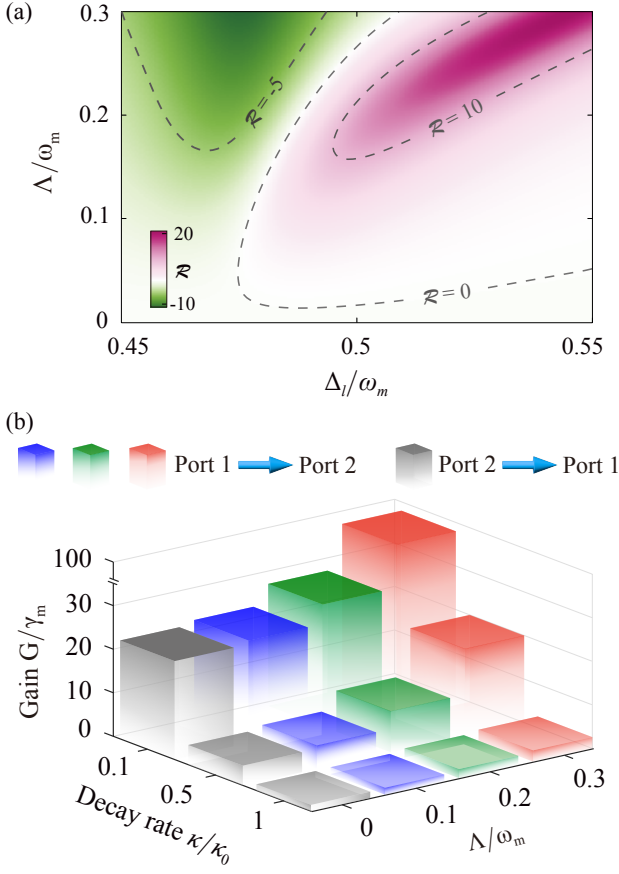


FIG. 4. (Color online) (a) Dependence of the isolation parameter \mathcal{R} on the detuning Δ_l and the squeezing strength Λ . (b) The optimal mechanical gain G versus the scaled decay rate κ/κ_0 and the squeezing strength Λ for different input directions, with the experimentally accessible parameter values $J_0/\omega_m = 0.48$ and $P_{\text{in}} = 10 \mu\text{W}$.

of the input drive field with the supermode ω_+ (i.e. driving the up energy level in Fig. 1(d)) [14–16]. In Figs. 3(b-d), we plot the dependence of mechanical gain G on input directions of the driving field. For the backward-input case, the maximum is located around $\Delta_l/\omega_m \sim 0.475$, corresponding to a backward phonon laser [see Fig. 3(a)]. However, for the forward-input case, the squeezing effect leads to a blueshift in the maximum of the mechanical gain G [see the orange dashed curve in Fig. 3(c) and the red solid curve in Fig. 3(d)]. That is, for $\Lambda/\omega_m = 0.3$, by driving the system from its left side (port 1 \rightarrow port 2), we can get maximum mechanical gain at $\Delta_l/\omega_m \sim 0.545$ [see Fig. 3(c)], corresponding to a forward phonon laser.

The underlying physical mechanism can be explained as follows: In the forward-input case, the squeezing effect causes a frequency shift to $a_{s,\cup}$ with respect to the bare mode $a_{2,\cup}$ [58], leading to $G/\gamma_m > 1$ around $\Delta_l/\omega_m \sim 0.545$. In contrast, in the backward-input case, the squeezing effect does not contribute anything to the $a_{2,\cup}$, corresponding to a conventional phonon laser ($G/\gamma_m > 1$ around $\Delta_l/\omega_m \sim 0.475$ with $J_0/\omega_m = 0.48$) [14–16]. This implies that, by adjusting the detuning Δ_l and squeezing strength Λ , one can get enhanced

or significantly suppressed mechanical gain by driving the device from the left or right side, or vice versa. Thus, our system provides a new route to realize a nonreciprocal phonon laser by changing the input directions. Compared with the method of using a rotating cavity to realize a nonreciprocal phonon laser [56, 57], our scheme only needs two-mode matching in one resonator, without its high-speed rotation, and is easier to realize experimentally. Thus, our work provides a new way to realize a nonreciprocal phonon laser.

According to Eq. (14), the stimulated emitted phonon number N_b can be calculated; that is,

$$N_b = \exp[2(G - \gamma_m)/\gamma_m], \quad (16)$$

which characterizes the performance of the phonon laser [14]. Then, from the above expression and under the threshold condition of phonon laser $N_b = 1$ (i.e., $G = \gamma_m$) [14], we can get the threshold pump power

$$P_{\text{th}} \approx \frac{2\hbar\kappa_0\gamma_m\omega_l[(J_s^2 + \kappa_0^2 - \Delta_l\Delta_s)^2 + \kappa_0^2(\Delta_s + \Delta_l)^2]}{\kappa_1 J_s g^2 x_0^2 \Delta_s}, \quad (17)$$

in which we have used $|b_s|^2 \ll 1$ at the threshold. It is clearly seen that the directional quantum squeezing effect has a significant impact on the threshold power P_{th} . In Fig. 3(e), we show the stimulated emitted phonon number N_b as a function of the pump power P_{in} . For the forward-input case (i.e., $\Lambda/\omega_m = 0.3$), the threshold power is about $7.2 \mu\text{W}$ at a fixed $\Delta_l/\omega_m = 0.545$ [corresponding to the maximal value of the mechanical gain in Fig. 3(d)], which approaches the threshold of about $7 \mu\text{W}$ reported in experiment [14]. In comparison, for the backward-input case (without the squeezing effect), the mechanical gain is suppressed at $\Delta_l/\omega_m = 0.545$, so a larger threshold power is required to implement the phonon laser.

To clearly see the squeezing effect on the nonreciprocal phonon lasing action, we introduce the isolation parameter

$$\mathcal{R} = 10 \log_{10} \frac{N_b(\Lambda \neq 0)}{N_b(\Lambda = 0)}, \quad (18)$$

where $N_b(\Lambda \neq 0)$ [or $N_b(\Lambda = 0)$] is the emitted phonon number corresponding to the forward-input case (or backward-input case). Figure 4(a) shows the isolation parameter \mathcal{R} versus the optical detuning Δ_l and the squeezing strength Λ . A nonzero isolation parameter \mathcal{R} indicates that nonreciprocity occurs in the phonon lasing action. It is found that when the detuning regions are selected correctly, nonreciprocity occurs. For example, for the detuning $\Delta_l/\omega_m \sim 0.545$ and squeezing strength $\Lambda/\omega_m = 0.3$, forward phonon lasing can be realized [see Figs. 3(b) and 3(d)], which is an inevitable result from the difference between $\delta n(\Lambda \neq 0)$ and $\delta n(\Lambda = 0)$. So, in such a COM system, nonreciprocal phonon lasing can be realized by directional quantum squeezing.

In experiments, the decay rate of the photon modes can be engineered, for example, by placing an external nanotip near a microresonator [95]. The effect of the normalized decay rate of photon mode κ/κ_0 on the optimal mechanical gain G for different input directions is shown in 4(b). It can be found that for the same value of squeezing strength Λ/ω_m , the optimal mechanical gain G of the forward-input case can reach a

TABLE I. Experimental parameters of the phonon laser in a coupled-microtoroid COM system

References	Resonators (Material)	Geometry	Diameter (μm)	Optical quality factors	Mechanical frequency (MHz)	Mechanical quality factors	Power threshold (μW)
[14]	R_1 (Si)	Microtoroid	$\sim 66 \mu\text{m}$	9.7×10^7	147.1	1×10^3	7
	R_2 (Si)	Microtoroid	$\sim 69 \mu\text{m}$	3×10^7	-	-	-
[15]	R_1 (Si)	Microtoroid	$\sim 68 \mu\text{m}$	9.25×10^7	59.2	18×10^3	1.2
	R_2 (Si)	Microtoroid	$\sim 69 \mu\text{m}$	2.5×10^7	-	-	-
[16]	R_1 (Si)	Microtoroid	$\sim 34.5 \mu\text{m}$	6.33×10^7	17.38	0.4×10^3	2.5
	R_2 (Si)	Microtoroid	$\sim 34 \mu\text{m}$	1.5×10^7	-	-	-

TABLE II. Performances of various $\chi^{(2)}$ -nonlinearity integrated mediums. PPLN: periodically poled LiNbO₃

References	Material	$\chi^{(2)}$ (pm/v)	Geometry	Size (μm): rings: $r/w/h$, disks: r/h , and spheres: r	Optical quality factor	Nonlinear single-photon coupling strength (MHz)	Pump power (mW)
[83]	PPLN	0.023	Microdisk	1500/500	2.0×10^8	-	25
[84]	LiNbO ₃	-	Microtoroid	1900/500	3.4×10^7	-	0.03
[85]	AlN	1.3	Microring	30/1.12/1.0	1.8×10^5	0.74	24.4
[86]	LiNbO ₃	2.1	Microdisk	51/0.7	1.1×10^5	-	10
[87]	SiO ₂	-	Microsphere	62	4.8×10^7	-	0.9
[88]	AlN	6	Microring	60/1.2/1.0	1.0×10^6	0.5	11
[89]	AlN	27	Microring	55/1.6/2	2.6×10^5	-	0.35
[90]	Si ₃ N ₄	0.2	Microring	23/1.2/0.6	1.2×10^6	-	15
[91]	Si ₃ N ₄	-	Microring	23/1.2/1.1	1.38×10^6	0.25	22.4
[92]	LiNbO ₃	0.6	Microring	80/1.6/0.6	9.0×10^5	-	20
[93]	PPLN	40	Microring	-	6.0×10^5	7.4	0.03
[94]	PPLN	-	Microring	75/-/-	1.8×10^6	1.2	0.1

much higher value than that of the opposite direction due to the directional quantum squeezing, indicating that the forward phonon laser tends to become more robust against decay rates of photon modes.

IV. EXPERIMENTAL FEASIBILITY

Phonon lasers have been demonstrated experimentally in a wide range of physical systems [9, 11–24]. In particular, optically pumped phonon lasing has been demonstrated in a compound COM system consisting of two coupled silica microtoroid WGM resonators and a nearby optical fiber [14–16]. As already confirmed in an experiment [14], the first resonator R_1 (with a diameter of $r_1 = 66 \mu\text{m}$) supports a high- Q ($Q_1 = 9 \times 10^7$) optical WGM mode and a mechanical mode with mechanical quality factor $Q_m = 1 \times 10^3$ and resonance frequency $\omega_m = 2\pi \times 23.4$ MHz. The second resonator R_2 (with a diameter of $r_2 = 69 \mu\text{m}$) supports a pure optical WGM mode with optical quality factor $Q_2 = 3 \times 10^7$. By placing a tapered optical fiber near the resonator, a tunable laser can be coupled into R_1 via the optical evanescent field. Also, the two resonators can be coupled through the evanescent field with the coupling strength J_0 , which can be adjusted by controlling the air gap between the resonators. For a controllable gap $0.2 \mu\text{m} \sim 2 \mu\text{m}$, J_0 is typically between 5 MHz \sim 5 GHz [14]. In such a COM system, when the upper state (supermode ω_+) is occupied by a sufficient number of photons coming from the driving laser through the nearby optical waveguide, these photons begin to split into the lower frequency photons of the lower state (supermode ω_-) and the coherent phonons, i.e., a

phonon amplifier and phonon laser with a power threshold of about $P_{\text{th}} = 7 \mu\text{W}$ [14]. As shown in Table I, we compare the performance of recent phonon laser experiments based on a composite COM system consisting of two coupled silica microtoroid WGM resonators and a nearby optical waveguide [14–16].

Recently, in experimental manufacturing [83–94], microring resonators with large $\chi^{(2)}$ -nonlinearity and high- Q can be fabricated using various thin film materials, such as silicon nitride, lithium niobate, and aluminum nitride. Table II shows more relevant parameters for experimentally achieving a $\chi^{(2)}$ -nonlinear resonator. We note that the Q factors of lithium-niobate-based resonators can reach 10^7 or 10^8 [83, 84, 86], which are better suited for our study. For an experimentally feasible quality factor $Q \simeq 4 \times 10^7$, the decay rate of a resonator with frequency $\omega_a = 1.93 \times 10^5$ GHz is $\kappa \simeq 48.2$ MHz. According to Eq. (27) (see Appendix A), the relationship between the power P_p of a pump field and the squeezing strength Λ is given by [58, 82]

$$\Lambda = \sqrt{8g_d^2\kappa_2 P_p / \hbar\omega_p\kappa_p^2}, \quad (19)$$

where g_d denotes nonlinear single-photon coupling strength in the parametric nonlinear process, and κ_p denotes the external decay rate for the pump field. By choosing experimentally feasible values [83–94]: $g_d = 0.025$ MHz, $\kappa_2 = 48.2$ MHz, $\kappa_p = 2\kappa_2$, and $\omega_p = 2\omega_a$. we choose pump power $P_p = 0.02 \mu\text{W}$ or $P_p = 30$ mW leading to $\Lambda/\omega_m \sim 0.2$ or $\Lambda/\omega_m \sim 290$. Therefore, we strongly believe that our proposed scheme is experimentally feasible.

V. CONCLUSION

In conclusion, we have studied a nonreciprocal phonon laser in a compound COM system consisting of an optomechanical resonator and a $\chi^{(2)}$ -nonlinear resonator. By unidirectionally pumping the nonlinear resonator, the squeezed effect occurs only in the selected direction, which significantly modifies the mechanical gain and power threshold, resulting in the nonreciprocal phonon lasing. Moreover, we find that in such nonreciprocal devices, the mechanical gain exhibits squeezing-enhanced robustness against optical decays. Our results opens up a new route to manipulate COM devices by using the directional quantum squeezing, and may find intriguing applications in designing phonon chips or high-precision motion sensors. Our scheme also opens many possibilities for further research: studying the role of directional quantum squeezing in enhancing or steering, for example, phonon blockade, macroscopic entanglement [96], and backscattering-immune force sensing [5], in which quantum noise terms should be included.

ACKNOWLEDGMENTS

H.J. is supported by the National Natural Science Foundation of China (NSFC, Grant No. 11935006), Hunan provincial major sci-tech program (2023ZJ1010), and the Science and Technology Innovation Program of Hunan Province (Grant No. 2020RC4047). L.-M.K. is supported by the NSFC (Grants No. 1217050862, 11935006 and 11775075). K.X. is supported by the National Key R&D Program of China (Grants No. 2019YFA0308704), the National Natural Science Foundation of China (Grants No. 92365107), and the Program for Innovative Talents and Teams in Jiangsu (Grant No. JSS-CTD202138). T.-X.L. is supported by the NSFC (Grant No. 12205054), the Jiangxi Provincial Education Office Natural Science Fund Project (GJJ211437), and Ph.D. Research Foundation (BSJJ202122). X.X. is supported by the NSFC (Grant No. 12265004). Y.W. is supported by the NSFC (Grant No. 12205256), and the Henan Provincial Science and Technology Research Project (Grant No. 232102221001).

APPENDIX A: DERIVATION OF THE HAMILTONIAN

We consider a compound COM system of two coupled resonators with the same resonance frequency ω_a . One of the resonators R_1 supports a mechanical breathing mode with frequency ω_m and effective mass m . The second resonator R_2 is a purely optical resonator that is coupled to the first resonator via an evanescent field with a coupling strength of J_0 . For simplicity, all directional subscripts are omitted. In the case of forward-input, the total Hamiltonian of this compound COM

system can be written as ($\hbar = 1$):

$$H' = \omega_a a_1^\dagger a_1 + \omega_a a_2^\dagger a_2 + \omega_m b^\dagger b + J_0(a_1^\dagger a_2 + a_2^\dagger a_1) + \omega_c c^\dagger c + g_d(a_2^{\dagger 2} c + a_2^2 c^\dagger) - g x_0 a_1^\dagger a_1 (b + b^\dagger) + i\varepsilon_l(a_1^\dagger e^{-i\omega_l t} - a_1 e^{i\omega_l t}) + i\lambda_p(c^\dagger e^{-i\omega_p t} - c e^{i\omega_p t}), \quad (20)$$

where ω_c is the frequency of the second-harmonic modes in R_2 . g and g_d are the COM coupling rate in the radiation-pressure process and the nonlinear single-photon coupling strength in the parametric nonlinear process. $\varepsilon_l = \sqrt{2\kappa_1 P_{\text{in}}/\hbar\omega_l}$ is the driving amplitude with input power P_{in} , $\lambda_p = \sqrt{2\kappa_2 P_p/\hbar\omega_p}$ is the pump light with the power P_p , here κ_1 and κ_2 are the decay rates. By using the unitary transformation $U = \exp\left[-i\frac{\omega_p}{2}a_1^\dagger a_1 - i\frac{\omega_p}{2}a_2^\dagger a_2 - i\omega_p c^\dagger c\right]t$, the Hamiltonian H' can be transformed into the rotating frame, i.e.,

$$H'' = U^\dagger H' U - iU^\dagger \frac{\partial U}{\partial t}. \quad (21)$$

Then we have

$$H'' = -\Delta' a_1^\dagger a_1 - \Delta' a_2^\dagger a_2 + \omega_m b^\dagger b + J_0(a_1^\dagger a_2 + a_2^\dagger a_1) - \Delta_c c^\dagger c + g_d(a_2^{\dagger 2} c + a_2^2 c^\dagger) - g x_0 a_1^\dagger a_1 (b + b^\dagger) + i\varepsilon_l(a_1^\dagger e^{-i\Delta_{\text{in}} t} - a_1 e^{i\Delta_{\text{in}} t}) + i\lambda_p(c^\dagger - c), \quad (22)$$

where $\Delta' = \omega_p/2 - \omega_a$, $\Delta_c = \omega_p - \omega_c$, and $\Delta_{\text{in}} = \omega_l - \omega_p/2$. The dynamical equation of c can be solved by the Heisenberg equation

$$\dot{c} = (i\Delta_c - \kappa_p)c + \lambda_p - ig_d a_2^2. \quad (23)$$

Here, we consider the strong pump field to excite mode c in R_2 [58]. Then we get the steady-state solution

$$c_s = \frac{-\lambda_p}{i\Delta_c - \kappa_p}. \quad (24)$$

After that, the Hamiltonian can be rewritten as

$$H'' = -\Delta' a_1^\dagger a_1 - \Delta' a_2^\dagger a_2 + \omega_m b^\dagger b + J_0(a_1^\dagger a_2 + a_2^\dagger a_1) - g x_0 a_1^\dagger a_1 (b + b^\dagger) + i\varepsilon_l(a_1^\dagger e^{-i\Delta_{\text{in}} t} - a_1 e^{i\Delta_{\text{in}} t}) + \frac{\Lambda}{2}(a_2^{\dagger 2} e^{-i\theta} + a_2^2 e^{i\theta}), \quad (25)$$

where the strength and the phase are

$$\Lambda = 2g_d \sqrt{\frac{2\kappa_2 P_p}{(\Delta_c^2 + \kappa_p^2)\hbar\omega_p}}, \quad \theta = -\text{Arg}(c_s). \quad (26)$$

Due to the resonance condition, we have $\omega_p = \omega_c$. Thus the pump power can be obtained as

$$P_p = \frac{\hbar\omega_p \kappa_p^2 \Lambda^2}{8g_d^2 \kappa_2}. \quad (27)$$

In a frame rotating at frequency Δ_{in} , the total Hamiltonian of this system can be written in the simplest level as

$$\mathcal{H} = -\Delta_l a_1^\dagger a_1 - \Delta_l a_2^\dagger a_2 + \omega_m b^\dagger b + J_0(a_1^\dagger a_2 + a_2^\dagger a_1) - g x_0 a_1^\dagger a_1 (b + b^\dagger) + i\varepsilon_l(a_1^\dagger - a_1) + \frac{\Lambda}{2}(a_2^{\dagger 2} e^{-i\theta} + a_2^2 e^{i\theta}), \quad (28)$$

where $\Delta_l = \Delta_{\text{in}} - \Delta' = \omega_l - \omega_1 = \omega_l - \omega_2$. To diagonalize \mathcal{H} , we define the squeezed operator a_s via the Bogoliubov transformation [59–61] $a_s = \cosh(r)a_2 + e^{-i\theta} \sinh(r)a_2^\dagger$, with the squeezing parameter $r = (1/4) \ln[(\Delta_l - \Lambda)/(\Delta_l + \Lambda)]$. The Hamiltonian \mathcal{H} can be rewritten as

$$\begin{aligned} \mathcal{H} = & -\Delta_l a_1^\dagger a_1 + \omega_m b^\dagger b - g x_0 a_1^\dagger a_1 (b + b^\dagger) \\ & - [\Delta_l (\cosh^2(r) + \sinh^2(r)) + 2\Lambda \cosh(r) \sinh(r)] a_s^\dagger a_s \\ & - \Delta_l \sinh^2(r) - \Lambda \cosh(r) \sinh(r) + i\varepsilon_l (a_1^\dagger - a_1) \\ & + J_0 \cosh(r) (a_1^\dagger a_s + a_s^\dagger a_1) \\ & - J_0 \sinh(r) (e^{-i\theta} a_1^\dagger a_s^\dagger + e^{i\theta} a_1 a_s). \end{aligned} \quad (29)$$

Then, with the rotating wave approximation and neglecting the constant term [59–61], the Hamiltonian of the system can be changed into

$$\begin{aligned} \mathcal{H} = & -\Delta_l a_1^\dagger a_1 - \Delta_s a_s^\dagger a_s + J_s (a_1^\dagger a_s + a_s^\dagger a_1) \\ & + \omega_m b^\dagger b - g x_0 a_1^\dagger a_1 (b + b^\dagger) + i\varepsilon_l (a_1^\dagger - a_1), \end{aligned} \quad (30)$$

where $\Delta_s = (\Delta_l + \Lambda) \exp(2r)$, $J_s = J_0 \cosh(r)$. This Hamiltonian sets the stage for our calculations of the mechanical gain and the threshold power in the forward-input case. For the backward-input case, we have $J_s = J_0$, and $\Delta_s = \Delta_l$. Then, the Heisenberg equations of motion are written as

$$\begin{aligned} \dot{a}_1 &= (i\Delta_l - \kappa_1) a_1 + i g x_0 (b + b^\dagger) a_1 - i J_s a_s + \varepsilon_l, \\ \dot{a}_s &= (i\Delta_s - \kappa_2) a_s - i J_s a_1, \\ \dot{b} &= -(i\omega_m + \gamma_m) b - i g x_0 a_1^\dagger a_1, \end{aligned} \quad (31)$$

where γ_m is the damping rate of the mechanical mode. As already confirmed in experiments with a COM-based phonon laser [14–16], for a strong driving field, the input noise terms can be safely ignored if one is interested only in the mean-number behaviors (i.e., the threshold feature of the mechanical gain or the phonon amplification). Then, the steady-state solutions can be obtained as

$$\begin{aligned} \alpha_1 &= \frac{\varepsilon_l (\kappa_2 - i\Delta_s)}{(\kappa_1 - i\Delta_l - i g x_s) (\kappa_2 - i\Delta_s) + J_s^2}, \\ \alpha_s &= \frac{J_s \alpha_1}{\Delta_s + i\kappa_2}, \quad \beta = \frac{g x_s |\alpha_1|^2}{\omega_m - i\gamma_m}, \end{aligned} \quad (32)$$

where $x_s = x_0 (\beta + \beta^*)$ is the steady-state mechanical displacement.

APPENDIX B: DERIVATION OF THE MECHANICAL GAIN

We introduce the supermode operators $a_\pm = (a_1 \pm a_s)/\sqrt{2}$, which satisfy the commutation relations $[a_+, a_+^\dagger] = [a_-, a_-^\dagger] = 1$, $[a_+, a_-^\dagger] = 0$. Eq. (30) can be written as

$$\begin{aligned} H = & \omega_+ a_+^\dagger a_+ + \omega_- a_-^\dagger a_- + \omega_m b^\dagger b, \\ & - \frac{g x_0}{2} [(a_+^\dagger a_+ + a_-^\dagger a_-) + (a_+^\dagger a_- + a_-^\dagger a_+)] (b^\dagger + b) \\ & + \frac{\Delta}{2} (a_+^\dagger a_- + a_-^\dagger a_+) + \frac{i\varepsilon_l}{\sqrt{2}} [(a_+^\dagger + a_-^\dagger) - (a_+ + a_-)], \end{aligned} \quad (33)$$

with the supermode frequencies $\omega_\pm = -(\Delta_s + \Delta_l)/2 \pm J_s$, and $\Delta = \Delta_s - \Delta_l$. Under the rotating-wave approximation condition $2J_s + \omega_m, \omega_m \gg |2J_s - \omega_m|$ [56, 57]. Thus we have

$$\begin{aligned} H = & \omega_+ a_+^\dagger a_+ + \omega_- a_-^\dagger a_- + \frac{\Delta}{2} (a_+^\dagger a_- + a_-^\dagger a_+) \\ & + \omega_m b^\dagger b - \frac{g x_0}{2} (a_+^\dagger a_- b + b^\dagger a_-^\dagger a_+) \\ & + \frac{i\varepsilon_l}{\sqrt{2}} [(a_+^\dagger + a_-^\dagger) - (a_+ + a_-)]. \end{aligned} \quad (34)$$

In the supermode picture, the dynamical equations of the system can be written as

$$\begin{aligned} \dot{a}_+ &= -(i\omega_+ + \kappa_0) a_+ + \frac{i}{2} (g x_0 b - \Delta) a_- + \frac{\varepsilon_l}{\sqrt{2}}, \\ \dot{a}_- &= -(i\omega_- + \kappa_0) a_- + \frac{i}{2} (g x_0 b^\dagger - \Delta) a_+ + \frac{\varepsilon_l}{\sqrt{2}}, \\ \dot{b} &= -(i\omega_m + \gamma_m) b + \frac{i g x_0}{2} a_+ a_-^\dagger, \end{aligned} \quad (35)$$

where $\kappa_0 = (\kappa_1 + \kappa_2)/2$. With the ladder operator $p = a_-^\dagger a_+$ and population inversion operator $\delta n = a_+^\dagger a_+ - a_-^\dagger a_-$, the dynamical equations of the system are then read

$$\begin{aligned} \dot{b} &= -(\gamma_m + i\omega_m) b + \frac{i g x_0}{2} p, \\ \dot{p} &= -2(\kappa_0 + iJ_s) p + \frac{i}{2} (\Delta - g x_0 b) \delta n + \frac{\varepsilon_l}{\sqrt{2}} (a_+ + a_-^\dagger). \end{aligned} \quad (36)$$

By setting the time derivatives of a_\pm and p as zero, we can solve the steady-state solutions of the system, i.e.,

$$\begin{aligned} p &= \frac{\sqrt{2} \varepsilon_l (a_+ + a_-^\dagger) - i (g x_0 b - \Delta) \delta n}{2i(2J_s - \omega_m) + 4\kappa_0}, \\ a_+ &= \frac{\varepsilon_l (2i\omega_- + 2\kappa_0 + i g x_0 b - i\Delta)}{2\sqrt{2} [D - i(\Delta_l + \Delta_s) \kappa_0]}, \\ a_- &= \frac{\varepsilon_l (2i\omega_+ + 2\kappa_0 + i g x_0 b^\dagger - i\Delta)}{2\sqrt{2} [D - i(\Delta_l + \Delta_s) \kappa_0]}, \end{aligned} \quad (38)$$

with

$$D = J_s^2 + \kappa_0^2 - \Delta_s \Delta_l + \frac{[g^2 x_0^2 n_b - 2g x_0 \Delta \text{Re}(b)]}{4},$$

where $n_b = b^\dagger b$. Substituting Eq. (38) into the dynamical equation of b in Eq. (36) results in

$$\dot{b} = (-i\omega_m - i\omega' + G - \gamma_m) b + F, \quad (39)$$

where

$$\begin{aligned} \omega' &= \frac{g^2 x_0^2 (2J_s - \omega_m) \delta n}{4(2J_s - \omega_m)^2 + 16\kappa_0^2} \\ &+ \frac{g^2 x_0^2 \varepsilon_l^2 \kappa_0^2 (\Delta_l + \Delta_s)}{[2(2J_s - \omega_m)^2 + 8\kappa_0^2] [D^2 + (\Delta_l + \Delta_s)^2 \kappa_0^2]}, \\ F &= \frac{g x_0 \Delta \delta n}{4i(2J_s - \omega_m) + 8\kappa_0} \\ &+ \frac{i g x_0 \varepsilon_l^2 [D(\kappa_0 - iJ_s) + \kappa_0(\Delta_l + \Delta_s)\Delta_s]}{[2i(2J_s - \omega_m) + 4\kappa_0] [D^2 + (\Delta_l + \Delta_s)^2 \kappa_0^2]}, \end{aligned}$$

and the mechanical gain is

$$\begin{aligned}
 G &= G_0 + \mathcal{G} \\
 &= \frac{g^2 x_0^2 \kappa_0 \delta n}{2(2J_s - \omega_m)^2 + 8\kappa_0^2} \\
 &\quad + \frac{\varepsilon_l^2 g^2 x_0^2 (\omega_m - 2J_s)(\Delta_s + \Delta_l) \kappa_0}{\left[4(2J_s - \omega_m)^2 + 16\kappa_0^2\right] \left[D^2 + (\Delta_l + \Delta_s)^2 \kappa_0^2\right]}, \quad (40)
 \end{aligned}$$

with

$$\delta n = \frac{\varepsilon_l^2 [2J_s \Delta_s - \kappa_0 g x_0 \text{Im}(b) - J_s g x_0 \text{Re}(b)]}{D^2 + \kappa_0^2 (\Delta_l + \Delta_s)^2}.$$

-
- [1] L. J. Swenson, A. Cruciani, A. Benoit, M. Roesch, C. S. Yung, A. Bideaud, and A. Monfardini, High-speed phonon imaging using frequency-multiplexed kinetic inductance detectors, *Appl. Phys. Lett.* **96**, 263511 (2010).
- [2] H. Shin, J. A. Cox, R. Jarecki, A. Starbuck, Z. Wang, and P. T. Rakich, Control of coherent information via on-chip photonic-phononic emitter-receivers, *Nat. Commun.* **6**, 6427 (2015).
- [3] A. Ganesan, C. Do, and A. Seshia, Phononic frequency comb via intrinsic three-wave mixing, *Phys. Rev. Lett.* **118**, 033903 (2017).
- [4] J. D. Cohen, S. M. Meenehan, G. S. MacCabe, S. Gröblacher, A. H. Safavi-Naeini, F. Marsili, M. D. Shaw, and O. Painter, Phonon counting and intensity interferometry of a nanomechanical resonator, *Nature* **520**, 522 (2015).
- [5] Y. He, Z. Feng, Y. Jing, W. Xiong, X. Chen, T. Kuang, G. Xiao, Z. Tan, and H. Luo, High-sensitivity force sensing using a phonon laser in an active levitated optomechanical system, *Opt. Express* **31**, 37507 (2023).
- [6] M. Serra-Garcia, V. Peri, R. Süssstrunk, O. R. Bilal, T. Larsen, L. G. Villanueva, and S. D. Huber, Observation of a phononic quadrupole topological insulator, *Nature* **555**, 342 (2018).
- [7] N. Li, J. Ren, L. Wang, G. Zhang, P. Hänggi, and B. Li, Colloquium: Phononics: Manipulating heat flow with electronic analogs and beyond, *Rev. Mod. Phys.* **84**, 1045 (2012).
- [8] R. Huang and H. Jing, The nanosphere phonon laser, *Nat. Photon.* **13**, 372 (2019).
- [9] K. Vahala, M. Herrmann, S. Knünz, V. Batteiger, G. Saathoff, T. W. Hänsch, and T. Udem, A phonon laser, *Nat. Phys.* **5**, 682 (2009).
- [10] T. Behrle, T. L. Nguyen, F. Reiter, D. Baur, B. de Neeve, M. Stadler, M. Marinelli, F. Lancellotti, S. F. Yelin, and J. P. Home, Phonon laser in the quantum regime, *Phys. Rev. Lett.* **131**, 043605 (2023).
- [11] J. T. Mendonça, H. Terças, G. Brodin, and M. Marklund, A phonon laser in ultra-cold matter, *Europhys. Lett.* **91**, 33001 (2010).
- [12] T. Kuang, R. Huang, W. Xiong, Y. Zuo, X. Han, F. Nori, C.-W. Qiu, H. Luo, H. Jing, and G. Xiao, Nonlinear multi-frequency phonon lasers with active levitated optomechanics, *Nat. Phys.* **19**, 414 (2023).
- [13] R. M. Pettit, W. Ge, P. Kumar, D. R. Luntz-Martin, J. T. Schultz, L. P. Neukirch, M. Bhattacharya, and A. N. Vamivakas, An optical tweezer phonon laser, *Nat. Photon.* **13**, 402 (2019).
- [14] I. S. Grudin, H. Lee, O. Painter, and K. J. Vahala, Phonon laser action in a tunable two-level system, *Phys. Rev. Lett.* **104**, 083901 (2010).
- [15] G. Wang, M. Zhao, Y. Qin, Z. Yin, X. Jiang, and M. Xiao, Demonstration of an ultra-low-threshold phonon laser with coupled microtoroid resonators in vacuum, *Photon. Res.* **5**, 73 (2017).
- [16] J. Zhang, B. Peng, Ş. K. Özdemir, K. Pichler, D. O. Krimer, G. Zhao, F. Nori, Y.-x. Liu, S. Rotter, and L. Yang, A phonon laser operating at an exceptional point, *Nat. Photon.* **12**, 479 (2018).
- [17] L. Mercadé, K. Pelka, R. Burgwal, A. Xuereb, A. Martínez, and E. Verhagen, Floquet phonon lasing in multimode optomechanical systems, *Phys. Rev. Lett.* **127**, 073601 (2021).
- [18] J. Sheng, X. Wei, C. Yang, and H. Wu, Self-organized synchronization of phonon lasers, *Phys. Rev. Lett.* **124**, 053604 (2020).
- [19] Q. Zhang, C. Yang, J. Sheng, and H. Wu, Dissipative coupling-induced phonon lasing, *Proc. Natl. Acad. Sci. U.S.A.* **119**, e2207543119 (2022).
- [20] I. Mahboob, K. Nishiguchi, A. Fujiwara, and H. Yamaguchi, Phonon lasing in an electromechanical resonator, *Phys. Rev. Lett.* **110**, 127202 (2013).
- [21] A. J. Kent, R. N. Kini, N. M. Stanton, M. Henini, B. A. Glavin, V. A. Kochelap, and T. L. Linnik, Acoustic phonon emission from a weakly coupled superlattice under vertical electron transport: Observation of phonon resonance, *Phys. Rev. Lett.* **96**, 215504 (2006).
- [22] R. P. Beardsley, A. V. Akimov, M. Henini, and A. J. Kent, Coherent terahertz sound amplification and spectral line narrowing in a stark ladder superlattice, *Phys. Rev. Lett.* **104**, 085501 (2010).
- [23] J. Kabuss, A. Carmele, T. Brandes, and A. Knorr, Optically driven quantum dots as source of coherent cavity phonons: A proposal for a phonon laser scheme, *Phys. Rev. Lett.* **109**, 054301 (2012).
- [24] A. Khaetskii, V. N. Golovach, X. Hu, and I. Žutić, Proposal for a phonon laser utilizing quantum-dot spin states, *Phys. Rev. Lett.* **111**, 186601 (2013).
- [25] N. Wang, H. Wen, J. C. A. Zacarias, J. E. Antonio-Lopez, Y. Zhang, D. C. Delgado, P. Sillard, A. Schülzgen, B. E. Saleh, R. Amezcuacorreia, and G. Li, Laser²/sup₂: A two-domain photon-phonon laser, *Sci. Adv.* **9**, eadg7841 (2023), <https://www.science.org/doi/pdf/10.1126/sciadv.adg7841>.
- [26] M. Aspelmeyer, T. J. Kippenberg, and F. Marquardt, Cavity optomechanics, *Rev. Mod. Phys.* **86**, 1391 (2014).
- [27] H. Jing, S. K. Özdemir, X.-Y. Lü, J. Zhang, L. Yang, and F. Nori, \mathcal{PT} -symmetric phonon laser, *Phys. Rev. Lett.* **113**, 053604 (2014).
- [28] Y. F. Xie, Z. Cao, B. He, and Q. Lin, \mathcal{PT} -symmetric phonon laser under gain saturation effect, *Opt. Express* **28**, 22580 (2020).
- [29] H. Lü, S. K. Özdemir, L.-M. Kuang, F. Nori, and H. Jing, Exceptional points in random-defect phonon lasers, *Phys. Rev. Appl.* **8**, 044020 (2017).
- [30] Y.-L. Zhang, C.-L. Zou, C.-S. Yang, H. Jing, C.-H. Dong, G.-C. Guo, and X.-B. Zou, Phase-controlled phonon laser, *New J. Phys.* **20**, 093005 (2018).

- [31] X.-Y. Zhang, C. Cao, Y.-P. Gao, L. Fan, R. Zhang, and C. Wang, Generation and manipulation of phonon lasing in a two-drive cavity magnomechanical system, *New J. Phys.* **25**, 053039 (2023).
- [32] B. Wang, Z.-X. Liu, X. Jia, H. Xiong, and Y. Wu, Polarization-based control of phonon laser action in a parity time-symmetric optomechanical system, *Commun. Phys.* **1**, 43 (2018).
- [33] B. Wang, H. Xiong, X. Jia, and Y. Wu, Phonon laser in the coupled vector cavity optomechanics, *Sci. Rep.* **8**, 282 (2018).
- [34] B. He, L. Yang, and M. Xiao, Dynamical phonon laser in coupled active-passive microresonators, *Phys. Rev. A* **94**, 031802 (2016).
- [35] Q. Lin, B. He, and M. Xiao, Catastrophic transition between dynamical patterns in a phonon laser, *Phys. Rev. Res.* **3**, L032018 (2021).
- [36] S. Kim, X. Xu, J. M. Taylor, and G. Bahl, Dynamically induced robust phonon transport and chiral cooling in an optomechanical system, *Nat. Commun.* **8**, 205 (2017).
- [37] H. Xu, L. Jiang, A. A. Clerk, and J. G. E. Harris, Nonreciprocal control and cooling of phonon modes in an optomechanical system, *Nature* **568**, 65 (2019).
- [38] D.-G. Lai, J.-F. Huang, X.-L. Yin, B.-P. Hou, W. Li, D. Vitali, F. Nori, and J.-Q. Liao, Nonreciprocal ground-state cooling of multiple mechanical resonators, *Phys. Rev. A* **102**, 011502 (2020).
- [39] R. Fleury, D. L. Sounas, C. F. Sieck, M. R. Haberman, and A. Alù, Sound isolation and giant linear nonreciprocity in a compact acoustic circulator, *Science* **343**, 516 (2014).
- [40] B.-I. Popa and S. A. Cummer, Non-reciprocal and highly nonlinear active acoustic metamaterials, *Nature Communications* **5**, 3398 (2014).
- [41] J. Zhang, B. Peng, Ş. K. Özdemir, Y.-x. Liu, H. Jing, X.-y. Lü, Y.-l. Liu, L. Yang, and F. Nori, Giant nonlinearity via breaking parity-time symmetry: A route to low-threshold phonon diodes, *Phys. Rev. B* **92**, 115407 (2015).
- [42] T. Devaux, V. Tournat, O. Richoux, and V. Pagneux, Asymmetric acoustic propagation of wave packets via the self-demodulation effect, *Phys. Rev. Lett.* **115**, 234301 (2015).
- [43] A. Seif, W. DeGottardi, K. Esfarjani, and M. Hafezi, Thermal management and non-reciprocal control of phonon flow via optomechanics, *Nat. Commun.* **9**, 1207 (2018).
- [44] B. Liang, X. S. Guo, J. Tu, D. Zhang, and J. C. Cheng, An acoustic rectifier, *Nature Materials* **9**, 989 (2010).
- [45] L. Shao, W. Mao, S. Maity, N. Sinclair, Y. Hu, L. Yang, and M. Lončar, Non-reciprocal transmission of microwave acoustic waves in nonlinear parity-time symmetric resonators, *Nat. Electron.* **3**, 267 (2020).
- [46] C. Coullais, D. Sounas, and A. Alù, Static non-reciprocity in mechanical metamaterials, *Nature* **542**, 461 (2017).
- [47] Y. Li, C. Shen, Y. Xie, J. Li, W. Wang, S. A. Cummer, and Y. Jing, Tunable asymmetric transmission via lossy acoustic metasurfaces, *Phys. Rev. Lett.* **119**, 035501 (2017).
- [48] Q. Wang, Z. Zhou, D. Liu, H. Ding, M. Gu, and Y. Li, Acoustic topological beam nonreciprocity via the rotational doppler effect, *Sci. Adv.* **8**, eabq4451 (2022).
- [49] G. Penelet, V. Pagneux, G. Poignand, C. Olivier, and Y. Aurégan, Broadband nonreciprocal acoustic scattering using a loudspeaker with asymmetric feedback, *Phys. Rev. Appl.* **16**, 064012 (2021).
- [50] X.-F. Li, X. Ni, L. Feng, M.-H. Lu, C. He, and Y.-F. Chen, Tunable unidirectional sound propagation through a sonic-crystal-based acoustic diode, *Phys. Rev. Lett.* **106**, 084301 (2011).
- [51] A. V. Poshakinskiy and A. N. Poddubny, Phonoritonic crystals with a synthetic magnetic field for an acoustic diode, *Phys. Rev. Lett.* **118**, 156801 (2017).
- [52] B. Li, Now you hear me, now you don't, *Nature Materials* **9**, 962 (2010).
- [53] S. A. Cummer, Selecting the direction of sound transmission, *Science* **343**, 495 (2014), <https://www.science.org/doi/pdf/10.1126/science.1249616>.
- [54] Y. Wang, B. Yousefzadeh, H. Chen, H. Nassar, G. Huang, and C. Daraio, Observation of nonreciprocal wave propagation in a dynamic phononic lattice, *Phys. Rev. Lett.* **121**, 194301 (2018).
- [55] R. Fleury, A. B. Khanikaev, and A. Alù, Floquet topological insulators for sound, *Nat. Commun.* **7**, 11744 (2016).
- [56] Y. Jiang, S. Maayani, T. Carmon, F. Nori, and H. Jing, Nonreciprocal phonon laser, *Phys. Rev. Appl.* **10**, 064037 (2018).
- [57] Y. Xu, J.-Y. Liu, W. Liu, and Y.-F. Xiao, Nonreciprocal phonon laser in a spinning microwave magnomechanical system, *Phys. Rev. A* **103**, 053501 (2021).
- [58] L. Tang, J. Tang, M. Chen, F. Nori, M. Xiao, and K. Xia, Quantum squeezing induced optical nonreciprocity, *Phys. Rev. Lett.* **128**, 083604 (2022).
- [59] X.-Y. Lü, Y. Wu, J. R. Johansson, H. Jing, J. Zhang, and F. Nori, Squeezed optomechanics with phase-matched amplification and dissipation, *Phys. Rev. Lett.* **114**, 093602 (2015).
- [60] W. Qin, V. Macri, A. Miranowicz, S. Savasta, and F. Nori, Emission of photon pairs by mechanical stimulation of the squeezed vacuum, *Phys. Rev. A* **100**, 062501 (2019).
- [61] W. Qin, A. Miranowicz, P.-B. Li, X.-Y. Lü, J. Q. You, and F. Nori, Exponentially enhanced light-matter interaction, cooperativities, and steady-state entanglement using parametric amplification, *Phys. Rev. Lett.* **120**, 093601 (2018).
- [62] W. Zhao, S.-D. Zhang, A. Miranowicz, and H. Jing, Weak-force sensing with squeezed optomechanics, *Sci. China-Phys. Mech. Astron.* **63**, 224211 (2019).
- [63] Y. Wang, C. Li, E. M. Sampuli, J. Song, Y. Jiang, and Y. Xia, Enhancement of coherent dipole coupling between two atoms via squeezing a cavity mode, *Phys. Rev. A* **99**, 023833 (2019).
- [64] C. J. Zhu, L. L. Ping, Y. P. Yang, and G. S. Agarwal, Squeezed light induced symmetry breaking superradiant phase transition, *Phys. Rev. Lett.* **124**, 073602 (2020).
- [65] Y. Wang, J.-L. Wu, J. Song, Z.-J. Zhang, Y.-Y. Jiang, and Y. Xia, Enhancing atom-field interaction in the reduced multiphoton tavis-cummings model, *Phys. Rev. A* **101**, 053826 (2020).
- [66] Y. Wang, J.-L. Wu, J.-X. Han, Y.-Y. Jiang, Y. Xia, and J. Song, Noise-resistant phase gates with amplitude modulation, *Phys. Rev. A* **102**, 032601 (2020).
- [67] W. Qin, A. Miranowicz, H. Jing, and F. Nori, Generating long-lived macroscopically distinct superposition states in atomic ensembles, *Phys. Rev. Lett.* **127**, 093602 (2021).
- [68] Y.-H. Chen, W. Qin, X. Wang, A. Miranowicz, and F. Nori, Shortcuts to adiabaticity for the quantum rabi model: Efficient generation of giant entangled cat states via parametric amplification, *Phys. Rev. Lett.* **126**, 023602 (2021).
- [69] M. Villiers, W. C. Smith, A. Petrescu, A. Borgognoni, M. Delbecq, A. Sarlette, M. Mirrahimi, P. Campagne-Ibarcq, T. Kontos, and Z. Leghtas, [arXiv:2212.04991](https://arxiv.org/abs/2212.04991).
- [70] W. Ge, B. C. Sawyer, J. W. Britton, K. Jacobs, J. J. Bollinger, and M. Foss-Feig, Trapped ion quantum information processing with squeezed phonons, *Phys. Rev. Lett.* **122**, 030501 (2019).
- [71] S. C. Burd, R. Srinivas, H. M. Knaack, W. Ge, A. C. Wilson, D. J. Wineland, D. Leibfried, J. J. Bollinger, D. Allcock, and D. Slichter, Quantum amplification of boson-mediated interactions, *Nat. Phys.* **17**, 898 (2021).
- [72] P.-B. Li, Y. Zhou, W.-B. Gao, and F. Nori, Enhancing spin-phonon and spin-spin interactions using linear resources in a hybrid quantum system, *Phys. Rev. Lett.* **125**, 153602 (2020).

- [73] M.-A. Lemonde, N. Didier, and A. A. Clerk, Enhanced nonlinear interactions in quantum optomechanics via mechanical amplification, *Nat. Commun.* **7**, 1 (2016).
- [74] Y. Wang, J.-L. Wu, J.-X. Han, Y. Xia, Y.-Y. Jiang, and J. Song, Enhanced phonon blockade in a weakly coupled hybrid system via mechanical parametric amplification, *Phys. Rev. Applied* **17**, 024009 (2022).
- [75] X.-F. Pan, X.-L. Hei, X.-L. Dong, J.-Q. Chen, C.-P. Shen, H. Ali, and P.-B. Li, Enhanced spin-mechanical interaction with levitated micromagnets, *Phys. Rev. A* **107**, 023722 (2023).
- [76] X.-L. Hei, P.-B. Li, X.-F. Pan, and F. Nori, Enhanced tripartite interactions in spin-magnon-mechanical hybrid systems, *Phys. Rev. Lett.* **130**, 073602 (2023).
- [77] Y. Wang, H.-L. Zhang, J.-L. Wu, J. Song, K. Yang, W. Qin, H. Jing, and L.-M. Kuang, Quantum parametric amplification of phonon-mediated magnon-spin interaction, *Sci. China-Phys. Mech. Astron.* **66**, 110311 (2023).
- [78] Y.-F. Jiao, Y.-L. Zuo, Y. Wang, W. Lu, J.-Q. Liao, L.-M. Kuang, and H. Jing, (2023), [arXiv:2311.11484](https://arxiv.org/abs/2311.11484).
- [79] C.-P. Shen, J.-Q. Chen, X.-F. Pan, Y.-M. Ren, X.-L. Dong, X.-L. Hei, Y.-F. Qiao, and P.-B. Li, Tunable nonreciprocal photon correlations induced by directional quantum squeezing, *Phys. Rev. A* **108**, 023716 (2023).
- [80] D.-Y. Wang, L.-L. Yan, S.-L. Su, C.-H. Bai, H.-F. Wang, and E. Liang, Squeezing-induced nonreciprocal photon blockade in an optomechanical microresonator, *Opt. Express* **31**, 22343 (2023).
- [81] D.-W. Liu, K.-W. Huang, Y. Wu, and L.-G. Si, Parametric amplification induced giant nonreciprocal unconventional photon blockade in a single microring resonator, *Appl. Phys. Lett.* **123**, 061103 (2023).
- [82] K.-W. Huang, Y. Wu, and L.-G. Si, Parametric-amplification-induced nonreciprocal magnon laser, *Opt. Lett.* **47**, 3311 (2022).
- [83] V. S. Ilchenko, A. A. Savchenkov, A. B. Matsko, and L. Maleki, Nonlinear optics and crystalline whispering gallery mode cavities, *Phys. Rev. Lett.* **92**, 043903 (2004).
- [84] J. U. Fürst, D. V. Strekalov, D. Elser, M. Lassen, U. L. Andersen, C. Marquardt, and G. Leuchs, Naturally phase-matched second-harmonic generation in a whispering-gallery-mode resonator, *Phys. Rev. Lett.* **104**, 153901 (2010).
- [85] X. Guo, C.-L. Zou, H. Jung, and H. X. Tang, On-chip strong coupling and efficient frequency conversion between telecom and visible optical modes, *Phys. Rev. Lett.* **117**, 123902 (2016).
- [86] J. Lin, Y. Xu, J. Ni, M. Wang, Z. Fang, L. Qiao, W. Fang, and Y. Cheng, Phase-matched second-harmonic generation in an on-chip LiNbO_3 microresonator, *Phys. Rev. Appl.* **6**, 014002 (2016).
- [87] X. Zhang, Q.-T. Cao, Z. Wang, Y.-x. Liu, C.-W. Qiu, L. Yang, Q. Gong, and Y.-F. Xiao, Symmetry-breaking-induced nonlinear optics at a microcavity surface, *Nat. Photon.* **13**, 21 (2019).
- [88] A. W. Bruch, X. Liu, J. B. Surya, C.-L. Zou, and H. X. Tang, On-chip $\chi^{(2)}$ microring optical parametric oscillator, *Optica* **6**, 1361 (2019).
- [89] Z. Ma, J.-Y. Chen, Z. Li, C. Tang, Y. M. Sua, H. Fan, and Y.-P. Huang, Ultrabright quantum photon sources on chip, *Phys. Rev. Lett.* **125**, 263602 (2020).
- [90] X. Lu, G. Moille, A. Rao, D. A. Westly, and K. Srinivasan, Efficient photoinduced second-harmonic generation in silicon nitride photonics, *Nat. Photon.* **15**, 131 (2021).
- [91] J.-Q. Wang, Y.-H. Yang, M. Li, X.-X. Hu, J. B. Surya, X.-B. Xu, C.-H. Dong, G.-C. Guo, H. X. Tang, and C.-L. Zou, Efficient frequency conversion in a degenerate $\chi^{(2)}$ microresonator, *Phys. Rev. Lett.* **126**, 133601 (2021).
- [92] Y. Xu, A. A. Sayem, L. Fan, C.-L. Zou, S. Wang, R. Cheng, W. Fu, L. Yang, M. Xu, and H. X. Tang, Bidirectional interconversion of microwave and light with thin-film lithium niobate, *Nat. Commun.* **12**, 4453 (2021).
- [93] J. Lu, A. A. Sayem, Z. Gong, J. B. Surya, C.-L. Zou, and H. X. Tang, Ultralow-threshold thin-film lithium niobate optical parametric oscillator, *Optica* **8**, 539 (2021).
- [94] J. Lu, M. Li, C.-L. Zou, A. A. Sayem, and H. X. Tang, Toward 1% single-photon anharmonicity with periodically poled lithium niobate microring resonators, *Optica* **7**, 1654 (2020).
- [95] B. Peng, Ş. Özdemir, S. Rotter, H. Yilmaz, M. Liertzer, F. Monifi, C. Bender, F. Nori, and L. Yang, Loss-induced suppression and revival of lasing, *Science* **346**, 328 (2014).
- [96] Y.-F. Jiao, S.-D. Zhang, Y.-L. Zhang, A. Miranowicz, L.-M. Kuang, and H. Jing, Nonreciprocal optomechanical entanglement against backscattering losses, *Phys. Rev. Lett.* **125**, 143605 (2020).